Solar Energy 188 (2019) 19–27

Contents lists available at ScienceDirect

Solar Energy

journal homepage: www.elsevier.com/locate/solener

A continuous input and output current quadratic buck-boost converter with positive output voltage for photovoltaic applications

Ali Sarikhani[a], Babak Allahverdinejad[a], Mohsen Hamzeh[b,*], Ebrahim Afjei[c]

[a] Faculty of Electrical Engineering, Shahid Beheshti University, Tehran, Iran
[b] School of Electrical and Computer Engineering, College of Engineering, University of Tehran, Tehran, Iran
[c] Department of Electrical Engineering, Shahid Beheshti University, Tehran, Iran

ARTICLE INFO

Keywords:
DC-DC converter
Renewable energy system
Small signal modeling
Solar power optimizer
Transformerless converter
Wide conversion ratio

ABSTRACT

This paper proposes a transformerless buck-boost DC-DC converter with positive output voltage. The voltage gain of the proposed buck-boost converter is square of voltage gain of conventional one. Therefore, the proposed converter can operate in a wide range of output voltage. Contrary to the conventional buck-boost converter, the proposed converter benefits from continuous input current, which makes it more suitable for renewable energy applications. Furthermore, the output current of the proposed converter is also continuous, which alleviates the current stress on the output capacitor and brings down the output voltage ripple. Principle operation, steady-state investigation, efficiency analysis and small signal modeling are addressed in detail for continuous conduction mode (CCM). Moreover, the proposed converter is compared to other quadratic buck-boost topologies in terms of different criteria. Finally, the performance of the proposed converter is verified through experimental results.

1. Introduction

As days go by, our planet encounters more and more perilous problems related to environmental pollution and climate change. Furthermore, demand for energy is rising so fast that sooner or later all fossil fuel resources will be depleted. It is noteworthy that a big deal of pollution on Earth is caused by excessive use of fossil fuels to produce energy, especially electricity. Therefore, it is necessary to find a substitute for this common resource of energy generation (Tewari and Sreedevi, 2018; Reshma Gopi and Sreejith, 2018). In recent years, the tendency toward renewable energies has significantly increased, since these resources are much more environmental friendly and cause much less harm to the planet Earth (Amir et al., 2018; Sarikhani et al., 2018; Trujillo et al., 2016).

The traditional technology in solar systems consists of PV panels and central inverters, as shown in Fig. 1(a). Since in these kind of systems, panels are connected in series and they draw equal current, one mismatch in any of these panels leads to huge power losses since there is only one central MPPT function for the whole system (Gokdag et al., 2018). Recent studies suggest distributed power point tracking (DMPPT) method in which MPPT is applied for each PV panel separately. In general, DMPPT can be divided into two groups, microinverters and solar power optimizers (SPOs). Microinverters, as depicted in Fig. 1(b), resolve issues related to systems with central inverters and increase the delivery power (Alluhaybi et al., 2019). However, the need for high step up voltage conversion may decrease the efficiency and moreover, complex topologies of microinverters increase the cost per watt. Fig. 1(c) illustrates a typical solar system with SPOs. In this concept, DC-DC converters play an important role, since they are responsible for delivering the highest power available from PV panels to the central inverter. Therefore, the better the performance of DC-DC converters, the higher the solar system efficiency (Tavassoli et al., 2017). The ability of stepping up and stepping down the output voltage is suitable for SPOs since PV panels undergo different weather conditions (SolarEdge Fixed String Voltage, 2019). As a result, Among DC-DC converters, buck-boost converters provide a better answer to applications in which a wide range of voltage conversion is required (MacAlpine et al., 2013; Vinnikov et al., 2018). Moreover, the buck-boost converters are highly utilized in many applications, such as industrial devices, electric vehicles and communication systems, which shows the importance of these types of converters (Jung et al., 2017; Hwu and Peng, 2012).

The conventional buck-boost converter has simple structure and benefits from high efficiency, but it suffers from discontinuous input

* Corresponding author.
E-mail addresses: al.sarikhani@Mail.sbu.ac.ir (A. Sarikhani), b.allahverdinejad@Mail.sbu.ac.ir (B. Allahverdinejad), mohsenhamzeh@ut.ac.ir (M. Hamzeh), e-afjei@sbu.ac.ir (E. Afjei).

https://doi.org/10.1016/j.solener.2019.05.025
Received 3 November 2018; Received in revised form 5 May 2019; Accepted 11 May 2019
Available online 01 June 2019
0038-092X/

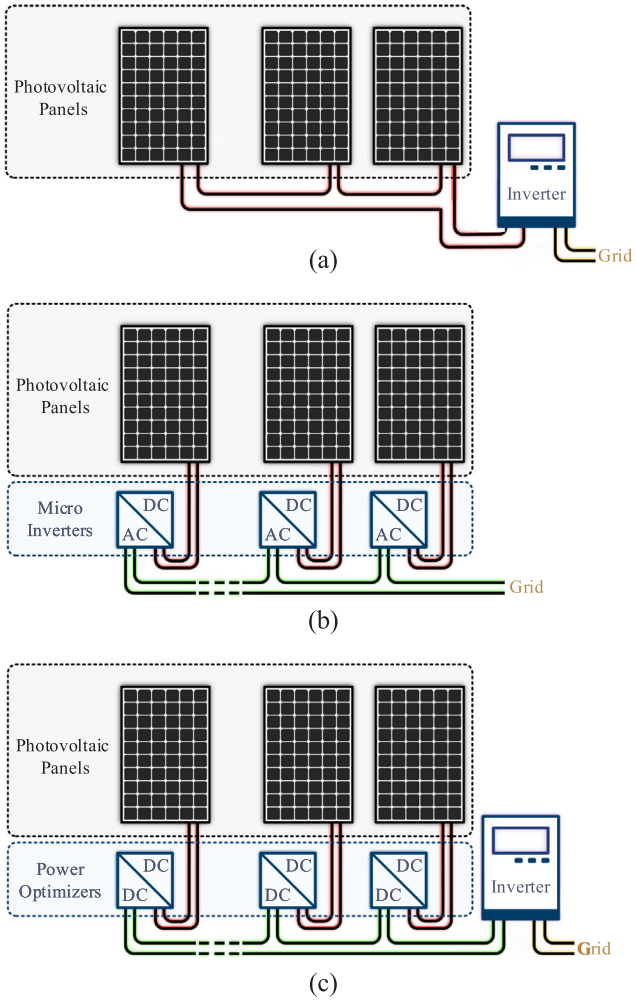

Fig. 1. Structure of grid-connected PV systems. (a) String technology, (b) Microinverter technology, (C) Solar power optimizer technology.

current and the limitation of voltage gain (Valdez-Resendiz et al., 2017; Banaei and Bonab, 2017). On the other hand, the quadratic buck-boost converter provides a wide range of voltage conversion ratio without extreme duty cycle (Gholizadeh et al., 2019). By cascading two conventional buck-boost converters, a quadratic buck-boost converter with positive output voltage is introduced in Maksimovic and Cuk (1989). Unfortunately, since the diodes clamp the input voltage to the output voltage, this converter can not operate appropriately when the duty cycle of the switch is greater than 0.5. By introducing an additional switch into the structure of conventional buck-boost converter, a quadratic buck-boost converter with positive output voltage is proposed in Miao et al. (2016). Although the converter has simple structure, it suffers from discontinuous input and output currents. It is worth mentioning that converters which have discontinuous input current are not suitable for renewable energy applications. Moreover, discontinuous output current increases the current stress on the output capacitor and exacerbates output voltage ripple. By merging one boost converter, one buck-boost converter and one buck converter, a single-switch quadratic buck-boost converter is presented in Zhang et al. (2018). This converter has continuous input current as well as continuous output current. The number of components used in this converter, especially the number of diodes, is relatively high, and it leads to a complex circuit topology and more power losses. Moreover, the output voltage polarity of this converter is negative. A quadratic buck-boost converter with zero output voltage ripple at a selectable operating point is introduced in Rosas-Caro et al. (2017). This converter has continuous input current and positive output voltage, but two floating power switches are required in its topology, which increases the cost of gate driver circuit.

In this paper, a quadratic buck-boost converter with positive output voltage is introduced which benefits from several aspects as:

- The proposed converter draws continuous input current which significantly reduces the filter requirement at input port and makes it more suited for renewable energy utilization.
- The proposed converter has continuous output current, which alleviates the current stress on the output capacitor and brings down the output voltage ripple.
- The presented converter can operate in a wide range of output voltage.
- Since the output voltage polarity of proposed converter is positive, common ground issue is settled.

The rest of the paper is arranged as follows. The proposed topology is presented, and the detailed operation principle and the efficiency analysis are explained in Section 2. The small signal modeling of the proposed converter is derived in Section 3. Section 4 draws a comparison among other quadratic buck-boost converters and the proposed converter. The experimental results of proposed converter are presented in Section 5, and conclusions are drawn in Section 6.

2. Proposed circuit topology and steady-state analysis

The proposed buck-boost converter is shown in Fig. 2. It consists of three inductors L_1, L_2 and L_3, three capacitors C_1, C_2 and C_O, two switches S_1 and S_2 and two diodes D_1 and D_2. The proposed converter is derived from combination of three basic conventional converters: boost converter, buck-boost converter and buck converter. The switches of proposed converter are turned ON and OFF simultaneously.

For simplification and facilitation, analysis is executed considering the following assumptions:

(1) Switches, diodes, inductors and capacitors are considered to be ideal.
(2) The voltage of capacitors is assumed to be constant.
(3) Analysis is done in continuous condition mode (CCM) and steady-sate.

1. *Mode 1*: During this mode, the switches S_1 and S_2 are turned ON concurrently whereas the diodes D_1 and D_2 are reverse-biased and are turned OFF. The inductors L_1, L_2 and L_3 are magnetized via the input source, capacitor C_1 and capacitor C_2, respectively. Therefore, capacitor C_1 and C_2 are discharged. It is worth mentioning that the current of S_2 is equal to $i_{L1} - i_{L3}$. Therefore, when $i_{L1} > i_{L3}$, the current flows from the switch S_2. Moreover, when $i_{L3} > i_{L1}$, the current flows from the body diode of the switch S_2. The current flow path of the proposed converter is demonstrated in Fig. 3(a). The differential equations of this mode can be derived as:

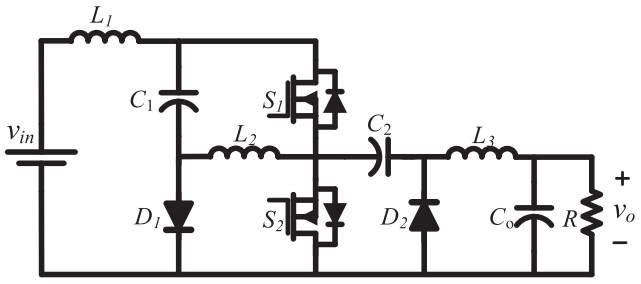

Fig. 2. Circuit diagram of the proposed quadratic buck-boost converter.

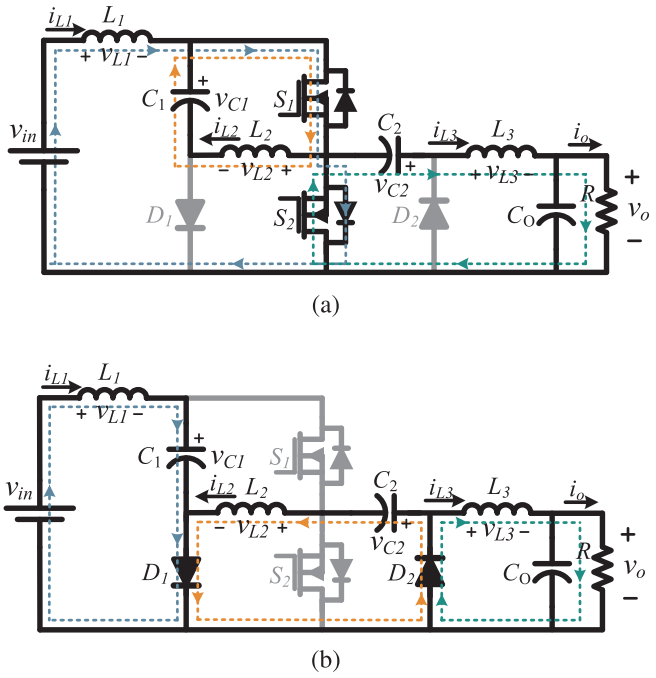

Fig. 3. The operation modes of proposed quadratic buck-boost converter. (a) Mode 1 and (b) Mode 2.

$$\begin{cases} L_1\frac{di_{L_1}}{dt} = v_{in} \\ L_2\frac{di_{L_2}}{dt} = v_{C1} \\ L_3\frac{di_{L_3}}{dt} = v_{C2} - v_O \end{cases} \quad \begin{cases} C_1\frac{dv_{C_1}}{dt} = -i_{L_2} \\ C_2\frac{dv_{C_2}}{dt} = -i_{L_3} \\ C_o\frac{dv_{C_o}}{dt} = i_{L_3} - \frac{v_o}{R}. \end{cases} \tag{1}$$

2. *Mode 2*: During this mode, The switches S_1 and S_2 are turned OFF simultaneously and the diodes D_1 and D_2 are forward-biased. The capacitor C_1 is charged by inductor L_1, and the stored energy in inductor L_2 is released into the capacitor C_2. Moreover, the inductor L_3 charges the capacitor C_o. In this mode, the voltages across the body diode of S_1 and S_2 are equal to $V_{C1} + V_{C2}$ and V_{C2}, respectively. As a result, the body diodes are reverse-biased and turned OFF. Fig. 3(b) illustrates the current flow path of proposed converter. The differential equations of this mode can be obtained as:

$$\begin{cases} L_1\frac{di_{L_1}}{dt} = v_{in} - v_{C1} \\ L_2\frac{di_{L_2}}{dt} = -v_{C2} \\ L_3\frac{di_{L_3}}{dt} = -v_O \end{cases} \quad \begin{cases} C_1\frac{dv_{C_1}}{dt} = i_{L_1} \\ C_2\frac{dv_{C_2}}{dt} = i_{L_2} \\ C_o\frac{dv_{C_o}}{dt} = i_{L_3} - \frac{v_o}{R}. \end{cases} \tag{2}$$

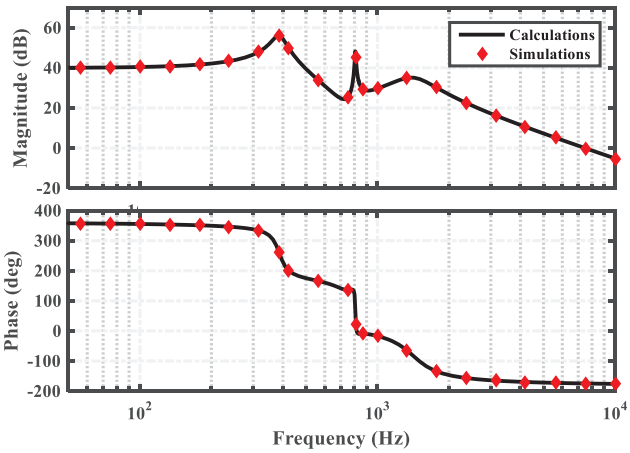

Fig. 5. Frequency response of control-to-output transfer function from small signal modeling and PLECS simulation.

By applying volt-second balance principle on the inductors L_1, L_2 and L_3, the voltage across the capacitors C_1 and C_2 and output capacitor can be easily calculated as:

$$\begin{cases} V_{C1} = \frac{1}{1-D}V_{in} \\ V_{C2} = \frac{D}{(1-D)^2}V_{in} \\ V_O = \left(\frac{D}{1-D}\right)^2 V_{in}. \end{cases} \tag{3}$$

Subsequently, the voltage gain of the proposed converter can be obtained as:

$$M = \frac{V_O}{V_{in}} = \left(\frac{D}{1-D}\right)^2. \tag{4}$$

It is distinct that the voltage conversion ratio of the introduced converter is square of that of the conventional buck-boost converter. Therefore, compared to conventional buck-boost converter, the proposed converter works in a wider range of output voltage, as shown in Fig. 4.

If the duty cycle of switches is less than 0.5, the proposed converter will work in step-down mode; otherwise, it will operate in step-up mode.

By applying ampere-second balance principle on the capacitors C_1, C_2 and C_O, the average current of inductors can be determined as

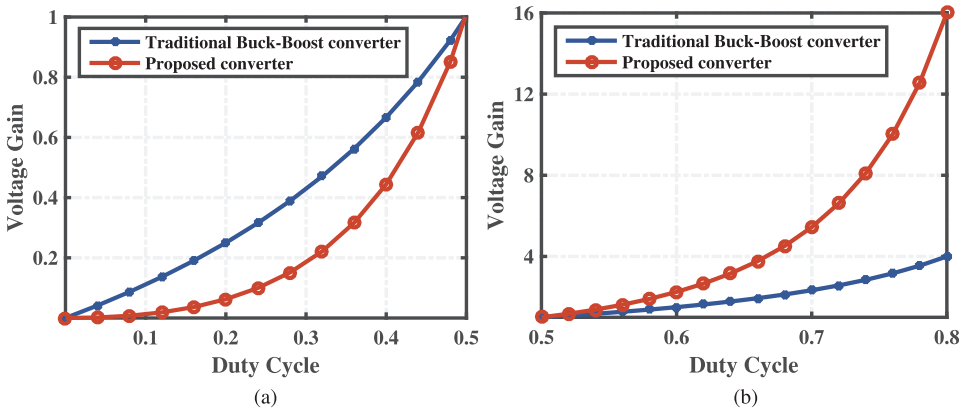

Fig. 4. Voltage gain versus duty cycle for the proposed converter and the conventional buck-boost converter. (a) Step-down mode. (b) Step-up mode.

Table 1
Comparison among existing quadratic buck-boost converters and proposed converter.

Topology	Miao et al. (2016)	Zhang et al. (2018)	Rosas-Caro et al. (2017)	Proposed
Inductor	2	3	2	3
Capacitor	2	3	2	3
Diode	2	5	2	2
Switch	2	1	2	2
Component	8	12	8	10
Voltage stress of switch (V_S/V_{in})	S_1 $\frac{1}{1-D}$ S_2 $\frac{D}{(1-D)^2}$	$\frac{1}{(1-D)^2}$	S_1 $\frac{1}{1-D}$ S_2 $\frac{D}{(1-D)^2}$	S_1 $\frac{1}{(1-D)^2}$ S_2 $\frac{D}{(1-D)^2}$
Voltage stress of diode (V_D/V_{in})	D_1 $\frac{1}{1-D}$ D_2 $\frac{D}{(1-D)^2}$	D_1 $\frac{1}{1-D}$ D_2 $\frac{D}{(1-D)^2}$ D_3 $\frac{1}{(1-D)^2}$ D_4 $\frac{1}{1-D}$ D_5 $\frac{D}{(1-D)^2}$	D_1 $\frac{1}{1-D}$ D_2 $\frac{D}{(1-D)^2}$	D_1 $\frac{1}{1-D}$ D_2 $\frac{D}{(1-D)^2}$
Continuous input current	No	Yes	Yes	Yes
Continuous output current	No	Yes	No	Yes
Output polarity	Positive	Negative	Positive	Positive
Experimental results (step-down)	V_{in}=18V V_o=8V I_o=0.8A η =76%	V_{in}=20V V_o=7V I_o=1.17A η =69%	*Not reported*	V_{in}=24V V_o=12V I_o=1A η =86.6%
Experimental results (step-up)	V_{in}=18V V_o=40.5V I_o=0.8A η =89%	V_{in}=20V V_o=38.7V I_o=0.65A η =83%	V_{in}=15V V_o=33V *Not reported*	V_{in}=24V V_o=48V I_o=1A η =90.9%

$$\begin{cases} I_{L1} = \left(\frac{D}{1-D}\right)^2 \frac{V_O}{R} \\ I_{L2} = \frac{D}{1-D}\frac{V_O}{R} \\ I_{L3} = \frac{V_O}{R}. \end{cases} \quad (5)$$

2.1. Voltage stresses of switches and diodes

From *Mode*1, the voltage stresses of the diodes can be calculated as:

$$\begin{cases} V_{D1} = \frac{1}{1-D} V_{in} \\ V_{D2} = \frac{D}{(1-D)^2} V_{in}. \end{cases} \quad (6)$$

Moreover, from *Mode*2 the voltage stresses of the power switches can be calculated as:

$$\begin{cases} V_{S1} = \frac{1}{(1-D)^2} V_{in} \\ V_{S2} = \frac{D}{(1-D)^2} V_{in}. \end{cases} \quad (7)$$

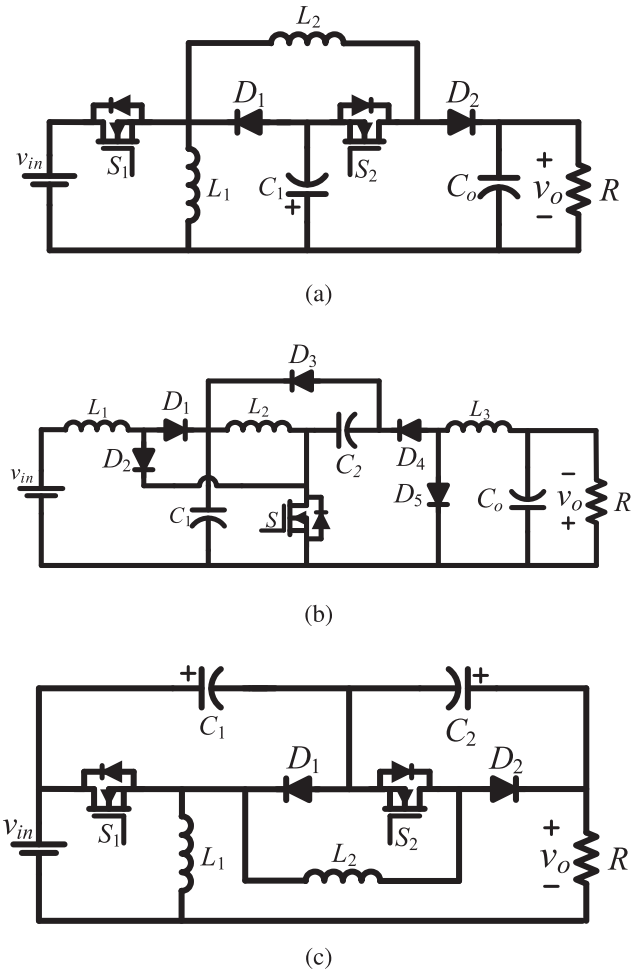

Fig. 6. Quadratic buck-boost converters. (a) Presented in Miao et al. (2016), (b) Presented in Zhang et al. (2018) and (c) Presented in Rosas-Caro et al. (2017).

2.2. Current stresses of switches and diodes

The current stresses of S_1 and S_2 can be found from

$$\begin{cases} I_{S1} = D(I_{L1} + I_{L2}) = \left(\frac{D}{1-D}\right)^2 \frac{V_o}{R} \\ I_{S2} = D(I_{L3} - I_{L1}) = \frac{D(1-2D)}{(1-D)^2}\frac{V_o}{R}. \end{cases} \quad (8)$$

From (8), it can be concluded that negative current of the switch S_2 will occur in step-up mode and the current flows through its body diode.

The current stresses of the diodes are obtained as:

$$\begin{cases} I_{D1} = (1-D)(I_{L1} + I_{L2}) = \frac{D}{1-D}\frac{V_o}{R} \\ I_{D2} = (1-D)(I_2 + I_3) = \frac{V_o}{R}. \end{cases} \quad (9)$$

2.3. Current ripple of inductors

From *Mode 1*, the current ripple of inductors is expressed as:

$$\begin{cases} \Delta I_{L1} = \frac{V_{L_1}}{L_1} DT_s = \frac{DV_{in}}{L_1 f_s} \\ \Delta I_{L2} = \frac{V_{L_2}}{L_2} DT_s = \frac{DV_{in}}{(1-D)L_2 f_s} \\ \Delta I_{L3} = \frac{V_{L_3}}{L_3} DT_s = \frac{D^2 V_{in}}{(1-D)L_3 f_s}, \end{cases} \quad (10)$$

where f_s is the switching frequency of the power switches.

To ascertain that all inductors work in CCM, the following

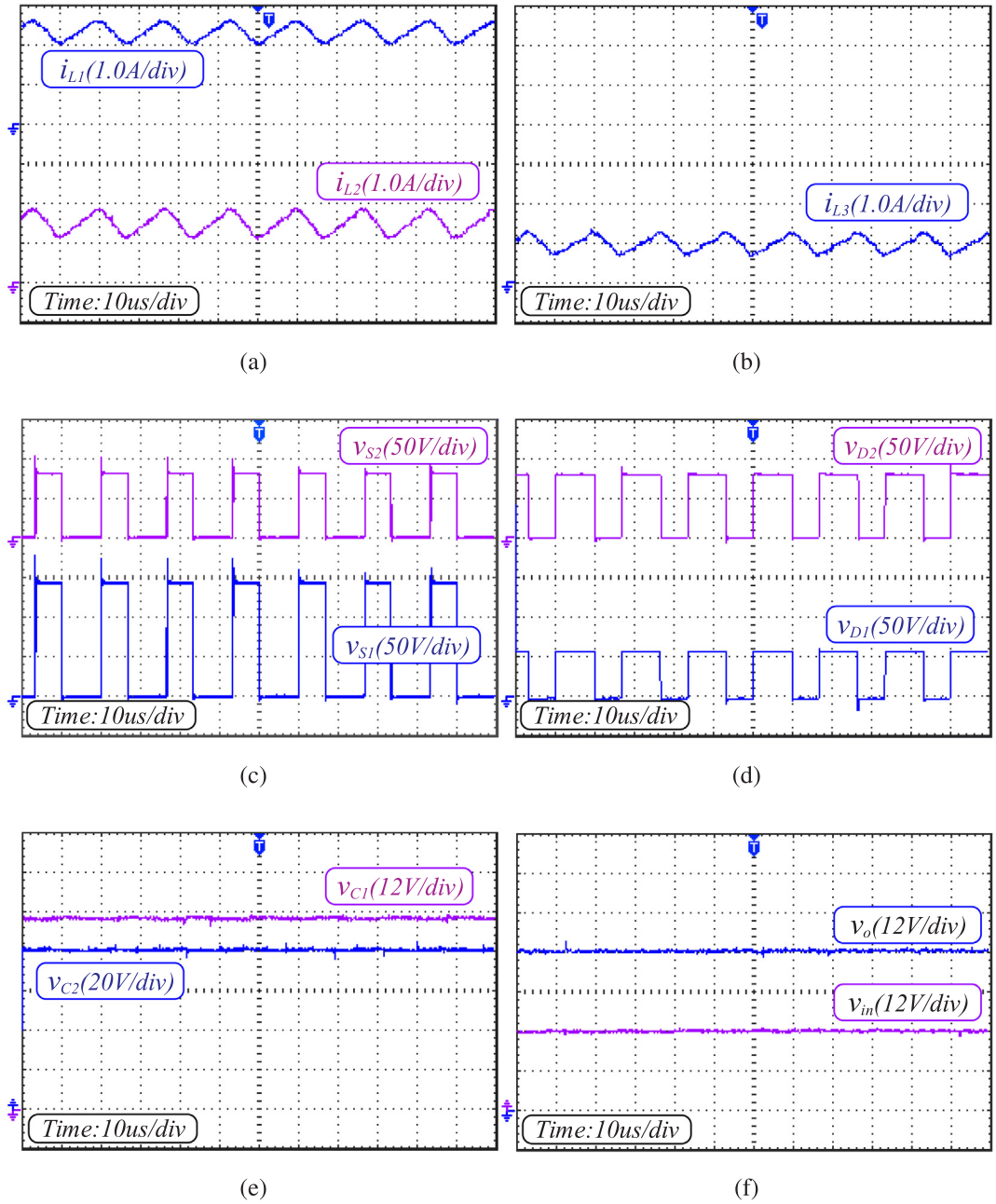

Fig. 7. Experimental results of propose converter in step-up mode. (a) Inductor currents i_{L1} and i_{L2}. (b) Inductor current i_{L3}. (c) Voltage stress of switches S_1 and S_2. (d) Voltage stress of diodes D_1 and D_2. (e) Capacitor voltage v_{C1} and v_{C2}. (f) Output and input voltages v_O and v_{in}.

conditions obtained from (5) and (10) must be satisfied:

$$\begin{cases} L_1 > \frac{(1-D)^4 R}{2D^3 f_s} \\ L_2 > \frac{(1-D)^2 R}{2D^2 f_s} \\ L_3 > \frac{(1-D)R}{2f_s}, \end{cases} \tag{11}$$

otherwise, the converter will operate in discontinuous current mode (DCM).

2.4. Voltage ripple of capacitors

The voltage ripple of the capacitors can be calculated as:

$$\begin{cases} \Delta V_{C1} = \frac{\Delta Q_{C1}}{C1} = \frac{D^2 V_o}{(1-D)RC1f_s} \\ \Delta V_{C2} = \frac{\Delta Q_{C2}}{C2} = \frac{DV_o}{RC2f_s} \\ \Delta V_o = \frac{\Delta Q_{Co}}{Co} = \frac{(1-D)V_o}{8L_3 Cof_s^2}. \end{cases} \tag{12}$$

Knowing D, f_s, V_o, R and allowable voltage ripple, appropriate capacitors can be selected.

2.5. Efficiency analysis

In order to facilitate efficiency analysis, voltage ripple of the capacitors and current ripple of inductors are neglected.

The total power loss of the switch S_1 is

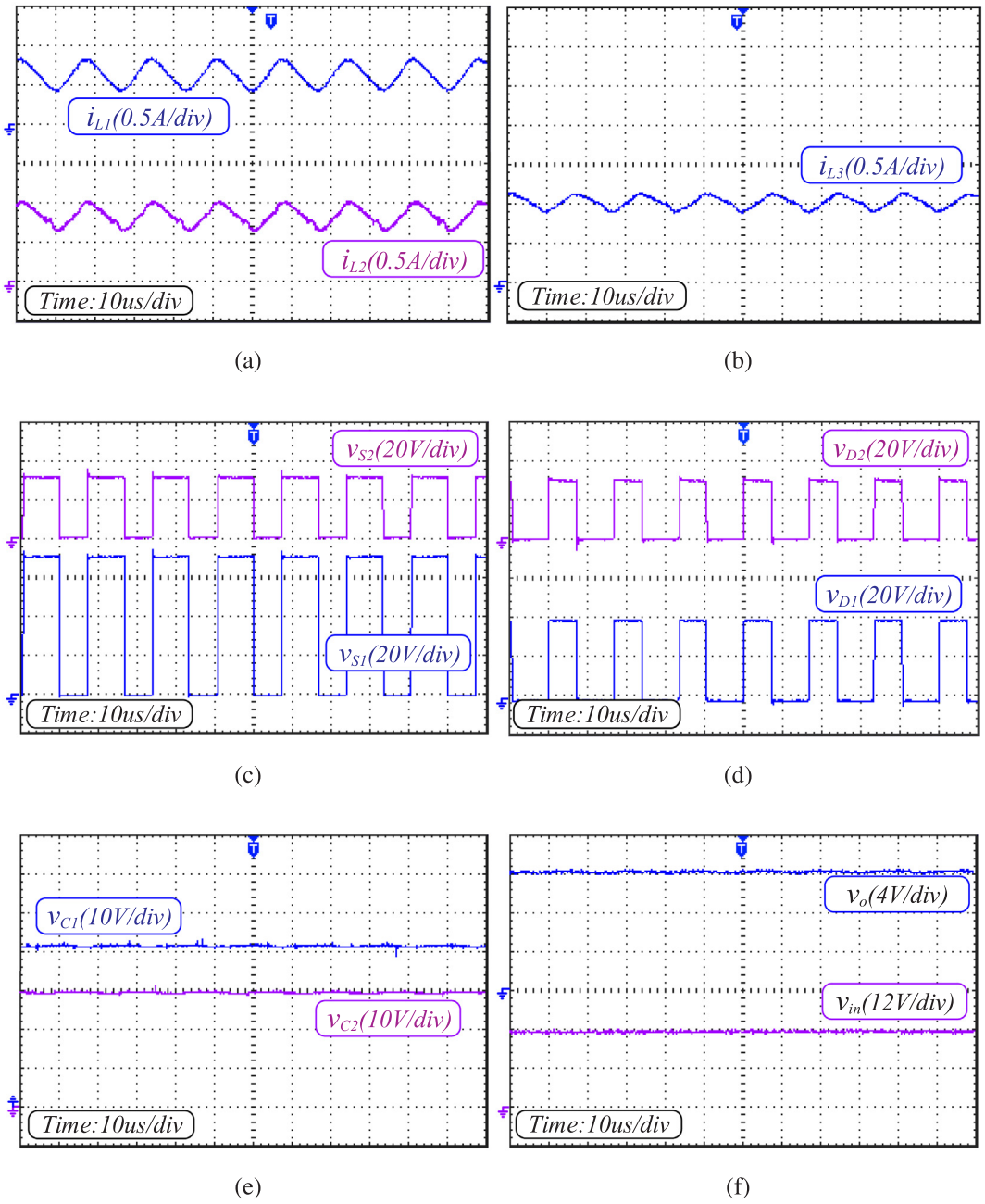

Fig. 8. Experimental results of propose converter in step-down mode. (a) Inductor currents i_{L1} and i_{L2}. (b) Inductor current i_{L3}. (c) Voltage stress of switches S_1 and S_2. (d) Voltage stress of diodes D_1 and D_2. (e) Capacitor voltage v_{C1} and v_{C2}. (f) Output and input voltages v_O and v_{in}.

$$P_{sw(S_1)}=P_{r_{DS1}}+P_{sw,off\,(S_1)}=r_{DS1}I_{S1,rms}^2+\frac{1}{2}I_{S1}V_{S1}t_{off_1}f_s=r_{DS1}\frac{D^3}{(1-D)^4}\frac{P_o}{R}+\frac{1}{2}\frac{P_o}{(1-D)}t_{off_1}f_s, \tag{13}$$

where r_{DS1} and t_{off1} are on-resistance and turn-off delay time of the switch S_1, respectively.

For step-down mode, the total losses of the switch S_2 are

$$P_{sw(S_2,step-down)}=P_{r_{DS2}}+P_{sw,off\,(S_2)}=r_{DS2}I_{S2,rms}^2+\frac{1}{2}I_{S2}V_{S2}t_{off_2}f_s=r_{DS2}\frac{D(1-2D)^2}{(1-D)^4}\frac{P_o}{R}+\frac{1}{2}\frac{(1-2D)P_o}{(1-D)^2}t_{off_2}f_s, \tag{14}$$

where r_{DS2} and t_{off2} are on-resistance and turn-off delay time of the switch S_2,respectively.

For step-up mode, the total loss of the switch S_2 are

$$P_{sw(S_2,step-up)}=r_{DS2}I_{S2,rms}^2+V_{FDS2}I_{S2}=r_{DS2}\frac{D(1-2D)^2}{(1-D)^4}\frac{P_o}{R}+V_{FDS2}\frac{D(1-2D)}{(1-D)^2}\frac{V_o}{R}, \tag{15}$$

where V_{FDS2} is the threshold voltage of body diode of the switch S_2.

The forward voltage losses of diodes D_1 and D_2 are obtained as:

$$P_{D_{VF}}=V_{FD1}I_{D1}+V_{FD2}I_{D2}=V_{FD1}\frac{DV_o}{(1-D)R}+V_{FD2}\frac{V_o}{R}, \tag{16}$$

where V_{FD1} and V_{FD2} are the threshold voltage of diodes D_1 and D_2, respectively.

The losses of inductors can be derived as below:

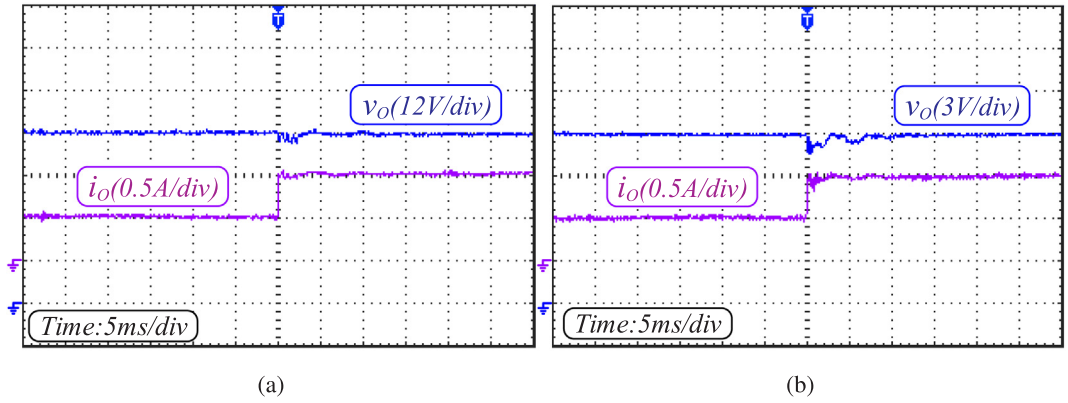

Fig. 9. Dynamic response of the proposed converter to the stepwise load increase. (a) Step-up mode. (b) Step-down mode.

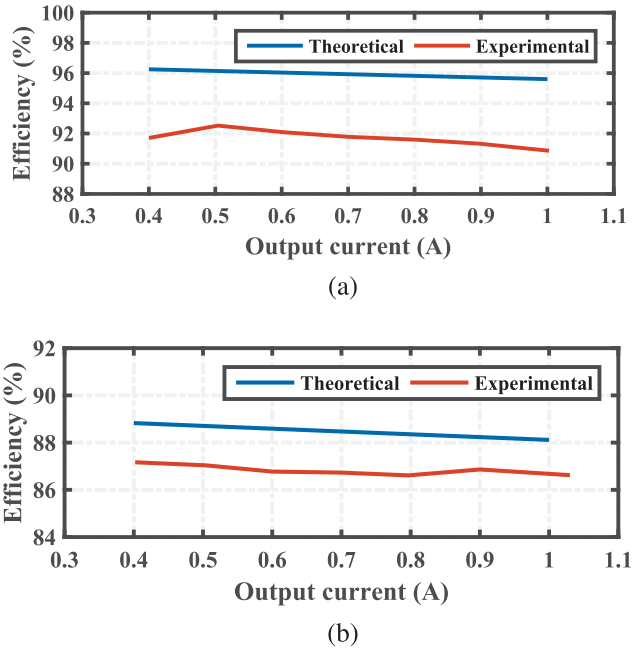

Fig. 10. Theoretical and experimental efficiency of proposed converter versus different output currents in (a) Step-up mode. (b) Step-down mode.

$$P_L = r_{L1} I_{L1,rms}^2 + r_{L2} I_{L2,rms}^2 + r_{L3} I_{L3,rms}^2 = r_{L1} \frac{D^4 P_o}{(1-D)^4 R} + r_{L2} \frac{D^2 P_o}{(1-D)^2 R} + r_{L3} \frac{P_o}{R}, \tag{17}$$

where r_{L1}, r_{L2} and r_{L3} are the equivalent series resistance, ESR, of L_1, L_2 and L_3, respectively.

The efficiency of the presented converter in step-down and step-up modes can be respectively written as:

$$\eta_{step-down} = \frac{P_o}{P_o + P_{sw(S1)} + P_{sw(S_2,step-down)} + P_{DVF} + P_L}, \tag{18}$$

and

$$\eta_{step-up} = \frac{P_o}{P_o + P_{sw(S1)} + P_{sw(S_2,step-up)} + P_{DVF} + P_L}. \tag{19}$$

3. Small signal modeling

In order to analyze the small-signal dynamics of the proposed converter, small-signal model of the converter should be derived. Based on averaging method (Middlebrook, 1988) and using (1) and (2), it can be written:

$$\begin{cases} L_1 \frac{d\langle i_{L1}\rangle}{dt} = \langle v_{in}\rangle - (1-d)\langle v_{C1}\rangle \\ L_2 \frac{d\langle i_{L2}\rangle}{dt} = d\langle v_{C1}\rangle - (1-d)\langle v_{C2}\rangle \\ L_3 \frac{d\langle i_{L3}\rangle}{dt} = d\langle v_{C2}\rangle - \langle v_o\rangle \\ C_1 \frac{d\langle v_{C1}\rangle}{dt} = (1-d)\langle i_{L1}\rangle - d\langle i_{L2}\rangle \\ C_2 \frac{d\langle v_{C2}\rangle}{dt} = (1-d)\langle i_{L2}\rangle - d\langle i_{L3}\rangle \\ C_o \frac{d\langle v_o\rangle}{dt} = \langle i_{L3}\rangle - \frac{\langle v_o\rangle}{R}, \end{cases} \tag{20}$$

where $\langle i_{L_1}\rangle$, $\langle i_{L_2}\rangle$, $\langle v_{C_1}\rangle$, $\langle v_{C_2}\rangle$, $\langle v_o\rangle$ are the average value of i_{L_1}, i_{L_2}, v_{C_1}, v_{C_2} and v_o, respectively, and d stands for the duty cycle.

Each averaged parameter, let's say $\langle x\rangle$, includes a DC value, X, and a small AC perturbation, $\hat{x}$. Hence, it can be expressed:

$$\begin{cases} \langle i_{L_1}\rangle = I_{L_1} + \hat{i}_{L_1} \\ \langle i_{L_2}\rangle = I_{L_2} + \hat{i}_{L_2} \\ \langle i_{L_3}\rangle = I_{L_3} + \hat{i}_{L_3} \\ \langle v_{C1}\rangle = V_{C1} + \hat{v}_{C1} \\ \langle v_{C2}\rangle = V_{C2} + \hat{v}_{C2} \\ \langle v_o\rangle = V_o + \hat{v}_o \\ d = D + \hat{d} \end{cases} \text{with} \quad \begin{cases} \hat{i}_{L1} \ll I_{L1} \\ \hat{i}_{L2} \ll I_{L2} \\ \hat{i}_{L3} \ll I_{L3} \\ \hat{v}_{C1} \ll V_{C1} \\ \hat{v}_{C2} \ll V_{C2} \\ \hat{v}_o \ll V_o \\ \hat{d} \ll D. \end{cases} \tag{21}$$

By substituting (21) into (20), and neglecting second order ac terms, the small signal model of the proposed converter can be determined as:

$$\begin{bmatrix} \frac{d\hat{i}_{L1}}{dt} \\ \frac{d\hat{i}_{L2}}{dt} \\ \frac{d\hat{i}_{L3}}{dt} \\ \frac{d\hat{v}_{C1}}{dt} \\ \frac{d\hat{v}_{C2}}{dt} \\ \frac{d\hat{v}_o}{dt} \end{bmatrix} = \begin{bmatrix} 0 & 0 & 0 & \frac{-(1-D)}{L_1} & 0 & 0 \\ 0 & 0 & 0 & \frac{D}{L_2} & \frac{-(1-D)}{L_2} & 0 \\ 0 & 0 & 0 & 0 & \frac{D}{L_3} & \frac{-1}{L_3} \\ \frac{1-D}{C_1} & \frac{-D}{C_1} & 0 & 0 & 0 & 0 \\ 0 & \frac{1-D}{C_2} & \frac{-D}{C_2} & 0 & 0 & 0 \\ 0 & 0 & \frac{1}{C_O} & 0 & 0 & \frac{-1}{RC_O} \end{bmatrix} \begin{bmatrix} \hat{i}_{L1} \\ \hat{i}_{L2} \\ \hat{i}_{L3} \\ \hat{v}_{C1} \\ \hat{v}_{C2} \\ \hat{v}_o \end{bmatrix} + \begin{bmatrix} \frac{V_{C1}}{L_1} \\ \frac{V_{C1}+V_{C2}}{L_2} \\ \frac{V_{C2}}{L_3} \\ -\frac{I_{L1}+I_{L2}}{C_1} \\ -\frac{I_{L2}+I_{L3}}{C_2} \\ 0 \end{bmatrix} \hat{d}. \tag{22}$$

By applying Laplace transform on (22), the control-to-output transfer function can be calculated, which plays an important role in design of the controller.

To confirm the accuracy of small signal modeling, frequency response of control-to-output transfer function from small signal modeling and PLECS simulation is depicted in Fig. 5. The parameters of the proposed converter are:

$L_1 = 365\ \mu$H, $L_2 = 900\ \mu$H, $L_3 = 615\ \mu$H.
$C_1 = 47\ \mu$F, $C_2 = 47\ \mu$F, $C_O = 22\ \mu$F.

$D = 41.42\%$, $V_{in} = 24\,V$, $V_O = 12\,V$, R = 12 Ω.

As observed in Fig. 5, theoretical calculation agrees with simulation result which confirms the correctness of small signal modeling.

4. Comparison

Table 1 shows the comparison among the converters presented in Miao et al. (2016), Zhang et al. (2018) and Rosas-Caro et al. (2017) illustrated in Fig. 6 and the proposed converter. The number of components, voltage stress on switches and diodes, input and output current type, output voltage polarity and experimental results are criteria of this comparison. All converters have quadratic voltage gain and can operate in step-down and step-up modes. The superiority of the converters presented in Miao et al. (2016) and Rosas-Caro et al. (2017) is due to having fewer number of components, but their output currents are discontinuous while the proposed converter and the converter presented in Zhang et al. (2018) have continuous current at input and output port which make them eminently suitable for renewable energy applications. In comparison to the converter presented in Zhang et al. (2018), the proposed converter requires one more switch and utilizes two less diodes. Furthermore, the output voltage of proposed converter is positive. Since in the proposed converter both switches have common source, only one isolated power supply is needed. On the other hand, in Miao et al. (2016) and Rosas-Caro et al. (2017), converters require two isolated power supply for driving the switches, which leads to an increase in costs, as seen in Fig. 6. The proposed converter, unlike the other ones, simultaneously has continuous input current, continuous output current and positive output voltage.

5. Experimental results

To confirm the performance and validity of the introduced converter, a prototype is built and tested. The designed parameters are selected as below:

$L_1 = 365\ \mu H$, $L_2 = 900\ \mu H$, $L_3 = 615\ \mu H$.
$r_{L1} = 0.026\ \Omega$, $r_{L2} = 0.14\ \Omega$, $r_{L3} = 0.064\ \Omega$,
$C_1 = 47\ \mu F$, $C_2 = 47\ \mu F$, $C_O = 22\ \mu F$.
$f_s = 60\,kHz$, $V_{in} = 24\,V$, $V_O = 12–48\,V$, R = 12–48 Ω.

It must be mentioned that these parameters are selected in accordance with the available equipment in the laboratory and safety reasons. Furthermore, the linear DC power supply GPS-2303 is utilized as input source. IRFB4227 and MUR840 are selected as switches and diodes, respectively. The TLP250 is used for gate driving circuit of the power switches. Current of inductors is measured with the current probe Tektronix A622. The time-domain waveforms are observed by the digital oscilloscope Agilent DSO3102A.

Some major waveforms of the presented converter are depicted in Fig. 7 in step-up mode. The currents of inductors L_1, L_2 and L_3 are shown in Fig. 7(a) and (b). Voltage stresses on S_1 and S_2 are depicted in Fig. 7c) and are equal to about 142 V and 82 V, which satisfies the expression (7). Fig. 7(d) shows voltage stresses on D_1 and D_2, which are about 59.6 V and 81 V. Fig. 7(e) illustrates the voltage across C_1 and C_2, which is in agreement with Eq. (3). Fig. 7(f) confirms that the output and input voltages are equal to 48 V and 24 V, respectively.

The experimental results of the introduced converter in step-down mode are demonstrated in Fig. 8. Fig. 8(a) and (b) illustrate the inductor currents. The voltage stresses of switches and diodes are depicted in Fig. 8(c) and (d), where $V_{S1} = 70.8\,V$ and $V_{S2} = 32\,V$. Fig. 7(e) indicates that the voltage of capacitors C_1 and C_2 is almost constant which is close to calculated values from (3). Moreover, the output and input voltages are shown in Fig. 7f) and are 12 V and 24 V.

To adjust the output voltage at desired value, the proposed converter is equipped with a PI controller. Fig. 9(a) and (b) show the dynamic response to the stepwise load increase in which the output load is changed from 96 Ω to 48 Ω and 24 Ω to 12 Ω in step-up and step-down modes, respectively. As observed, the proposed converter responds well to load change with suitable dynamics.

Fig. 10(a) and (b) show the theoretical and experimental efficiencies versus output current of the introduced converter in step-up and step-down mode, respectively. In the rated power, the experimental efficiency in step-up and step-down mode is equal to 90.9% and 86.6%, respectively. It is possible to improve the overall efficiency of the presented converter via utilizing better components.

6. Conclusion

In this paper, a transformerless buck-boost DC-DC converter is introduced. The principle operation and steady-state analysis of proposed converter are presented in the CCM circuit operation. Moreover, small signal modeling is addressed, which is verified through PLECS simulation. The proposed converter is implemented and tested in step-up and step-down modes and its performance has been verified through the experimental results. The proposed converter benefits from several merits as continuous input and output currents. This contributes to smaller filter size at input and output ports. Moreover, the presented converter has positive output voltage polarity and quadratic voltage gain. The introduced converter is a suitable nominee for renewable applications, especially as SPOs and utilizing in industrial systems.

References

Alluhaybi, K., Batarseh, I., Hu, H., Chen, X., 2019. Comprehensive Review and Comparison of Single-Phase Grid-Tied Photovoltaic Microinverters. IEEE J. Emerg. Sel. Top. Power Electron.

Amir, A., Che, H.S., Amir, A., Khateb, A.E., Rahim, N.A., 2018. Transformerless high gain boost and buck-boost DC-DC converters based on extendable switched capacitor (SC) cell for stand-alone photovoltaic system. Sol. Energy 171, 212–222.

Banaei, M.R., Bonab, H.A.F., 2017. A novel structure for single-switch nonisolated transformerless buck-boost DC–DC converter. IEEE Trans. Industr. Electron. 64 (1), 198–205.

Gholizadeh, H., Sarikhani, A., Hamzeh, M., 2019. A transformerless quadratic buck-boost converter suitable for renewable applications. In: 10th International Power Electronics, Drive Systems and Technologies Conference (PEDSTC), Shiraz, Iran, pp. 470–474.

Gokdag, M., Akbaba, M., Gulbudak, O., 2018. Switched-capacitor converter for PV modules under partial shading and mismatch conditions. Sol. Energy 170, 723–731.

Hwu, K.I., Peng, T.J., 2012. A novel buck-boost converter combining KY and buck converters. IEEE Trans. Power Electron. 27 (5), 2236–2241.

Jung, Y.H., Hong, S.K., Kwon, O.K., 2017.. high-efficient and fast-transient buck-boost converter using adaptive direct path skipping and on-duty modulation. Microelectron. J. 70, 43–51.

MacAlpine, S.M., Erickson, R.W., Brandemuehl, M.J., 2013. Characterization of power optimizer potential to increase energy capture in photovoltaic systems operating under nonuniform conditions. IEEE Trans. Power Electron. 28 (6), 2936–2945.

Maksimovic, D., Cuk, S., 1989. General properties and synthesis of PWM DC-to-DC converters. In: IEEE Power Electronics Specialists Conference, pp. 515–525.

Miao, S., Wang, F., Ma, X., 2016. A New Transformerless Buck-Boost Converter With Positive Output Voltage. IEEE Trans. Industr. Electron. 63 (5), 2965–2975.

Middlebrook, R.D., 1988. Small signal modeling of pulse-width modulated switched-mode power converters. Proc. IEEE 76 (4), 343–354.

Reshma Gopi, R., Sreejith, S., 2018. Converter topologies in photovoltaic applications – A review. Renew. Sustain. Energy Rev. 94, 1–14.

Rosas-Caro, Julio C., Sanchez, Victor M., Valdez-Resendiz, Jesus E., Mayo-Maldonado, Jonathan C., Beltran-Carbajal, Francisco, Valderrabano-Gonzalez, Antonio, 2017. Quadratic buck–boost converter with positive output voltage and continuous input current for PEMFC systems. Int. J. Hydrogen Energy 42 (51), 30400–30406.

Sarikhani, A., Allahverdinejad, B., Torkaman, H., 2018. A non-isolated buck-boost DC-DC converter with single switch. In: 9th Annual Power Electronics, Drives Systems and Technologies Conference (PEDSTC), Tehran, pp. 369–373.

SolarEdge Fixed String Voltage, Concept of Operation, 2019. [Online]. Available: https://www.solaredge.com.

Tavassoli, A., Allahverdinejad, B., Rashidirad, N., Hamzeh, M., 2017. Performance analysis of series SPOs in a droop-controlled DC microgrid. In: Smart Grid Conference (SGC), Tehran, pp. 1–6.

Tewari, N., Sreedevi, V.T., 2018. A novel single switch dc-dc converter with high voltage gain capability for solar PV based power generation systems. Sol. Energy 171, 466–477.

Trujillo, C.L., Santamaría, F., Gaona, E.E., 2016. Modeling and testing of two-stage grid-connected photovoltaic micro-inverters. Renew. Energy 99, 533–542.

Valdez-Resendiz, Jesus E., Sanchez, Victor M., Rosas-Caro, Julio C., Mayo-Maldonado,

Jonathan C., Sierra, J.M., Barbosa, Romeli, 2017. Continuous input-current buck-boost DC-DC converter for PEM fuel cell applications. Int. J. Hydrogen Energy 42 (51), 30389–30399.
Vinnikov, D., Chub, A., Liivik, L., Kosenko, R., Korkh, O., 2018. Solar Optiverter - A novel hybrid approach to the photovoltaic module level power electronics. IEEE Trans. Industr. Electron.
Zhang, N., Zhang, G., See, K.W., Zhang, B., 2018. A single-switch quadratic buck-boost converter with continuous input port current and continuous output port current. IEEE Trans. Power Electron. 33 (5), 4157–4166.